

Superconducting and normal-state interlayer-exchange-coupling in $\text{La}_{0.67}\text{Sr}_{0.33}\text{MnO}_3$ - $\text{YBa}_2\text{Cu}_3\text{O}_7$ - $\text{La}_{0.67}\text{Sr}_{0.33}\text{MnO}_3$ epitaxial trilayers.

K. Senapati and R. C. Budhani*

Department of Physics, Indian Institute of Technology Kanpur, Kanpur - 208016, India

(Dated: March 23, 2022)

The issue of interlayer exchange coupling in magnetic multilayers with superconducting (SC) spacer is addressed in $\text{La}_{0.67}\text{Sr}_{0.33}\text{MnO}_3$ (LSMO) - $\text{YBa}_2\text{Cu}_3\text{O}_7$ (YBCO) - $\text{La}_{0.67}\text{Sr}_{0.33}\text{MnO}_3$ (LSMO) epitaxial trilayers through resistivity, ac-susceptibility and magnetization measurements. The ferromagnetic (FM) LSMO layers possessing in-plane magnetization suppress the critical temperature (T_c) of the c-axis oriented YBCO thin film spacer. The superconducting order, however, survives even in very thin layers (thickness $d_Y \sim 50 \text{ \AA}$, ~ 4 unit cells) at $T < 25 \text{ K}$. A predominantly antiferromagnetic (AF) exchange coupling between the moments of the LSMO layers at fields $< 200 \text{ Oe}$ is seen in the normal as well as the superconducting states of the YBCO spacer. The exchange energy J_1 ($\sim 0.08 \text{ erg/cm}^2$ at 150 K for $d_Y = 75 \text{ \AA}$) grows on cooling down to T_c , followed by truncation of this growth on entering the superconducting state. The coupling energy J_1 at a fixed temperature drops exponentially with the thickness of the YBCO layer. The temperature and d_Y dependencies of this primarily non-oscillatory J_1 are consistent with the coupling theories for systems in which transport is controlled by tunneling. The truncation of the monotonic T dependence of J_1 below T_c suggests inhibition of single electron tunneling across the CuO_2 planes as the in-plane gap parameter acquires a non-zero value.

PACS numbers: 74.78.Fk, 75.60.-d, 75.70.Cn

I. INTRODUCTION

The oscillatory nature of exchange coupling between two ferromagnetic (FM) layers separated by a metallic but non-magnetic (NM) spacer as a function of the spacer thickness d_n is now well established in a variety of systems^{1,2,3,4,5,6,7}. It is generally agreed that the coupling is driven by the Ruderman-Kittel-Kasuya-Yoshida (RKKY)-type exchange through the conduction electrons of the spacer¹. The period of oscillations predicted by the theories of exchange coupling is directly related to the extremal wave vectors connecting opposite sides of the Fermi Surface (FS) of the spacer material in the direction of the layer growth. Clearly, the nature of the Fermi surface of the spacer plays a key role in interlayer exchange. Šipr and Györfy⁸ first suggested that an experiment in which the Fermi surface could be changed while keeping all other material parameters the same, would allow a direct test of the exchange coupling theories based on extremal wave vectors of the FS. They proposed the use of a superconducting (SC) spacer in which an isotropic gap opens up at the FS on cooling below the critical temperature T_c . The zero-temperature numerical calculations of Šipr and Györfy⁸ show that the oscillatory coupling is strongly damped in the presence of a superconducting gap. Similarly, the analytical results of de Melo^{9,10} show that at $\Delta/T \gg 1$ the coupling decays exponentially as $\exp(-k_{FS}d_s\Delta/E_F)$, where k_{FS} , d_s , Δ and E_F are the Fermi wave-vector, spacer thickness, gap parameter and Fermi energy respectively. Near T_c the large thermally excited quasiparticle density compensates for the loss of coupling seen at low temperatures.

Experimental verification of these predictions is, however, constrained by several materials related factors.

First of all, since the oscillatory coupling is seen only when the spacer thickness is small ($\leq 130 \text{ \AA}$), one must ensure that superconductivity survives in such thin spacers in the presence of the strong pair-breaking effects of the ferromagnetic boundaries. Naturally, short coherence length ξ_0 and high critical temperature T_c of the superconductor, and small exchange energy of the ferromagnet are the desirable features to see the effect. In addition, one must also ensure that the interfaces between the ferromagnetic and superconducting layers are atomically smooth.

The doped Mott insulators of the perovskite oxide family meet some of these material specifications. For example, $\text{YBa}_2\text{Cu}_3\text{O}_7$ (YBCO) superconductor and $\text{La}_{0.67}\text{Sr}_{0.33}\text{MnO}_3$ (LSMO) ferromagnet can be grown epitaxially on top of each other. The cuprate has anisotropic but short coherence length and a high T_c , whereas the manganite with a Curie temperature of $\approx 360 \text{ K}$, has relatively small exchange energy J ($\sim 1 \text{ meV}$) as compared to the J of 3d transition metal ferromagnets such as Fe and Co which are strong pair-breakers¹¹. However, the cuprates also pose interesting challenges, such as the nodal gap parameters Δ and anomalous c-axis transport, not present in elemental superconductors. Reported measurements on high T_c superconductor (HTSC)-manganite heterostructures have primarily focused on the suppression of T_c ^{12,13,14}, spin injection^{15,16,17} and the effects on magnetoresistance^{18,19}. Recently, the aspect of exchange coupling across HTSC layers has been addressed by Przyslupski et al.²⁰ using $(\text{La}_{0.67}\text{Sr}_{0.33}\text{MnO}_3)_n/(\text{YBa}_2\text{Cu}_3\text{O}_7)_m$ multilayers where $n = 16$ unit cells, and m varies from 1 to 8 unit cells. Measurements of field-cooled (FC) and zero-field-cooled

(ZFC) magnetization loops in these samples reveal exchange biasing effects, which have been argued to be an indicator of interlayer exchange coupling. However, this work also attributes the shift of the FC and ZFC loops to antiferromagnetism in LSMO. Here it needs to be pointed out that these multilayers have been deposited on LaAlO_3 substrates, which introduce large compressive stress in LSMO and YBCO epitaxial films due to its smaller lattice parameter (~ 3.79 Å). In addition, LaAlO_3 is a heavily twinned material. Since both these factors are known to affect magnetic anisotropy of LSMO²¹ and superconducting properties of YBCO²², intrinsic behavior of FM-SC-FM structure is likely to get masked by such stress and interface related effects. Further, the interface related non-intrinsic behavior is likely to get accentuated in superlattices due to the presence of a large number of interfaces in such structures.

Here we report the magnetic behavior of LSMO-YBCO-LSMO trilayers, synthesized on [001] SrTiO_3 substrates. The lattice parameter of SrTiO_3 (~ 3.91 Å) compares well with the lattice parameter of $\text{La}_{0.67}\text{Sr}_{0.33}\text{MnO}_3$ (~ 3.89 Å) and the average ab-plane lattice spacing of $\text{YBa}_2\text{Cu}_3\text{O}_7$ (~ 3.85 Å). The scope for a stress-free layer-by-layer growth has been improved further through special chemical treatment of the substrate²³. We first describe the magnetic behavior of plane LSMO films of various thickness. High quality epitaxial layers of LSMO showing a soft magnetic character and in-plane anisotropy were integrated with YBCO in a trilayer form and the superconducting critical temperature of such structures was measured. The suppression in T_c has been attributed to the pair breaking effects at the FM-SC boundary. Finally, the issue of interlayer exchange coupling has been addressed through measurements of ZFC in-plane magnetization loops over a broad range of temperatures. These measurements reveal a long range antiferromagnetic coupling between LSMO layers decaying exponentially with the thickness of the YBCO spacer.

II. EXPERIMENTAL

Thin films of LSMO, and trilayers of LSMO-YBCO-LSMO and $\text{PrBa}_2\text{Cu}_3\text{O}_7$ - $\text{YBa}_2\text{Cu}_3\text{O}_7$ - $\text{PrBa}_2\text{Cu}_3\text{O}_7$ (PBCO-YBCO-PBCO) were deposited on chemically polished [001] oriented SrTiO_3 substrates. A multitarget pulsed laser deposition technique based on KrF excimer laser ($\lambda = 248$ nm) was used to deposit the films and trilayers at 800 °C and 200 mTorr O_2 partial pressure²⁴. Since the growth conditions for all three oxides were identical, the trilayers were deposited sequentially without changing the process parameters. A slow deposition rate (~ 1 Å/sec) established through several calibration runs, was used to realize a layer-by-layer growth of LSMO, PBCO, and YBCO. While for the plane LSMO films we have studied the changes in transport and magnetic properties as a function of thickness from 50 Å to 1100 Å, the thickness of each LSMO layer in LSMO-YBCO-LSMO

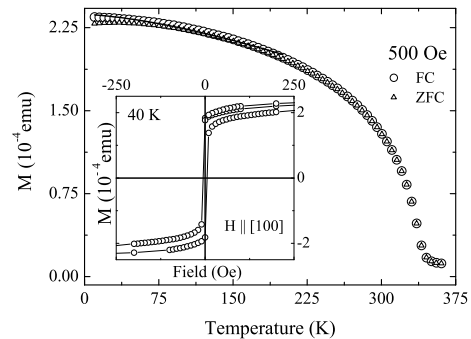


FIG. 1: Zero-field-cooled (Δ) and field-cooled (O) magnetization of a 600 Å thick film of $\text{La}_{0.67}\text{Sr}_{0.33}\text{MnO}_3$ measured with 500 Oe in-plane field directed along the [100] axis. The solid line is a fit to the field-cooled curve using the Bloch law (Eq. 1) for the decay of magnetization at $T \ll T_c$. Inset: Zero-field-cooled hysteresis loop of the same film measured at 40 K in the same configuration as the measurement of $M(T)$.

trilayers was fixed at 300 Å, and the thickness of the cuprate was varied from 50 Å to 300 Å. For the PBCO-YBCO-PBCO trilayers, a constant PBCO layer thickness of 100 Å was used. The crystallographic structure of the films was characterized with $\theta-2\theta$ X-ray diffraction. The SC and FM critical temperatures of the films were established through resistivity $\rho(T)$, ac-susceptibility $\chi(T)$ and magnetization $M(T)$ measurements. We have used a home-built micro-Hall-probe based ac-susceptometer²⁵ for detailed measurements of vortex dynamics in these films²⁴. The measurements of resistivity in the temperature range of 2 K to 370 K were carried out in the standard four-probe geometry. A superconducting quantum interference device (SQUID) based magnetometer (MPMS-XL5) operated in the RSO mode for higher sensitivity was used for detailed measurements of zero-field-cooled and field-cooled magnetization and M-H loops. The magnetic field in these measurements was in the plane of the film, aligned along one of the principal axes ([100] or [010]). Measurements were also performed with the field in the [110] direction to check for the in-plane anisotropy of magnetization.

III. RESULTS

A. Magnetic ordering in thin $\text{La}_{0.67}\text{Sr}_{0.33}\text{MnO}_3$ films:

Figure 1 shows the ZFC and FC magnetization of a 600 Å thick LSMO film measured at 500 Oe. The onset of spontaneous magnetization at ~ 350 K on cooling marks the Curie temperature of the sample. The ZFC and FC branches of magnetization in granular and multi-domain magnetic films of large coercivity show a pronounced bifurcation at lower temperatures. In the

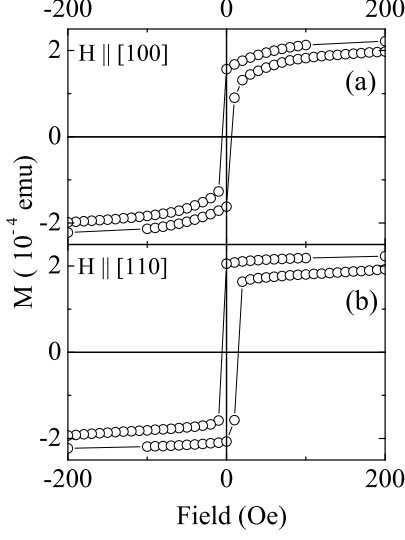


FIG. 2: Zero-field-cooled magnetization loops at 100 K measured with in-plane applied field along the [100] (panel ‘a’) and [110] (panel ‘b’) directions. In both cases the data are corrected for a small diamagnetic contribution from the STO substrate.

present case, however, the two branches nearly superimpose down to the lowest temperature. This feature indicates the growth of a defect-free magnetic film of low coercivity. We analyze the temperature dependence of the FC magnetization in the framework of the Bloch theory for decay of magnetization due to excitation of spin waves²⁶. The drop in saturation magnetization is predicted to be of the form;

$$M_s(T)/M_s(0) = 1 - AT^{3/2} \quad (1)$$

Here $M_s(0)$ is the saturation magnetization at $T = 0$, and the coefficient A is expressed as $(C/S)(k_B/2JS)^{3/2}$, where $C = 0.059$ for a simple cubic magnetic lattice, S the total spin and J the exchange integral which is given by the formula $k_B T_c/J = (5/96)(Z-1)[11S(S+1)-1]$ of Rushbrooke and Wood²⁷. An excellent fit to the magnetization at $T \ll T_{Curie}$ is seen with a dependence of the type $1 - AT^{3/2}$, when the average spin $S (= 1.835)$ per Mn site is used. The exchange energy deduced from the fits is ~ 2 meV, while the exchange energy of the strong ferromagnets like Fe is ~ 5.5 meV deduced from a Bloch constant of $\sim 3.6 \times 10^{-6} \text{ deg}^{-3/2}$.

In order to check for a preferred in-plane axis of magnetization, we have measured the hysteresis loops with the external field aligned along the [100] and [110] directions of the [001] oriented films. Results of this measurement are shown in Fig. 2(a, b). A perfect hysteresis loop with the remanent magnetization (M_r) equal to M_s is seen when the field is along [110]. Whereas in the

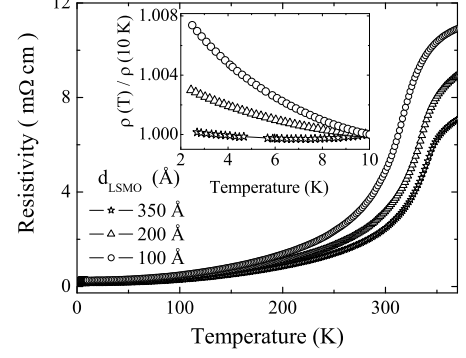


FIG. 3: Resistivity ($\rho(T)$) of LSMO films deposited on STO in the temperature range of 2 K - 370 K. Thickness of the films varies from 100 Å to 350 Å. Inset shows a magnified view of the low temperature section of the $\rho(T)$ curves. These data have been normalized with respect to the resistivity at 10 K in order to emphasize the upturn in the resistivity of the thinnest films.

case of $H \parallel [100]$ (Fig. 2a), $M_r = M_s/\sqrt{2}$. This observation clearly indicates that [110] is the easy axis of magnetization and [100] is the hard axis. However, the small value of the switching field suggests that the energy barrier for rotation of magnetization is not large. This result is consistent with the earlier measurements of magnetization loops in films of LSMO deposited on STO substrates^{28,29}. The square hysteresis loops seen in the figure further suggest that these films are magnetically quite soft. The behavior of magnetization in LSMO films deposited on LAO is quite different. The preferred direction of magnetization is perpendicular to the film plane in this case^{21,30,31}.

Unlike the other double exchange manganites such as $\text{La}_{0.67}\text{Ca}_{0.33}\text{MnO}_3$, the resistivity of LSMO with 30 to 40 % Sr is metallic in the paramagnetic state³². This metallic conduction is seen in our films as well. The resistivity of these films at room temperature is low ($\sim 2 \text{ m}\Omega \text{ cm}$), and remains metallic down to 2 K. Fig. 3 displays the zero-field resistivity of LSMO films spanning over a thickness range of 100 Å to 350 Å in the temperature window of 2 K - 370 K. The paramagnetic metallic phase above T_{Curie} which transits to a ferromagnetic metallic phase at $T < T_{Curie}$, is clearly identifiable for all films. T_{Curie} acquires the near bulk value (~ 350 K) for films thicker than 200 Å, while thinner films show a slight drop in the Curie temperature. The resistivity at the lowest temperature normalized with respect to its value at 10 K, is shown in the inset of Fig. 3. A small upturn in resistivity, which can be attributed to weak localization and electron-electron interaction effects in 2D, is observed only for the thinnest films (≤ 200 Å). These features indicate the growth of a high quality thin film of LSMO. The magnetic and electrical characteristics of LSMO dominate the behavior of $\rho(T)$ and $M(T)$ in

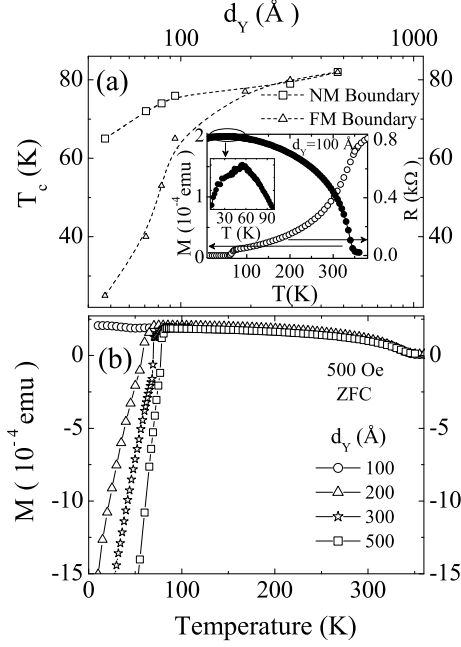


FIG. 4: Panel (a) : T_c (open symbols) plotted as a function of d_Y in LSMO-YBCO-LSMO and PBCO-YBCO-PBCO trilayers. Inset shows $R(T)$ and zero-field-cooled $M(T)$ of a LSMO-YBCO-LSMO sample with $d_Y = 100$ Å. An enlarged view of $M(T)$ near T_c is also shown. Panel (b): Temperature dependence of the zero-field-cooled magnetization of LSMO-YBCO-LSMO trilayers with 100, 200, 300 and 500 Å thick SC layers. The measurement field of 500 Oe was applied along the [100] direction in the plane of the films.

LSMO-YBCO-LSMO trilayers at $T > 100$ K as described in the following section.

B. Superconductivity in LSMO - YBCO - LSMO trilayers:

In the inset of Fig. 4(a) we plot the magnetization and resistivity of a LSMO-YBCO-LSMO trilayer with YBCO layer thickness (d_Y) of 100 Å. At $T \leq 360$ K a metallic behavior is evident in the resistivity plot. This becomes pronounced at $T < T_{Curie}$. At lower temperatures however, the resistance of the sample drops to zero as the current path is shorted by the superconducting YBCO layer. Correspondingly, there is a non-zero diamagnetic contribution to magnetization due to the Meissner effect. In trilayers with thicker YBCO film, the magnetization actually crosses the zero-line and becomes negative. This is seen in Fig. 4(b) where we have plotted the ZFC magnetization of some trilayers with different YBCO thickness. The superconducting transition temperature (T_c) in these heterostructures is a strong function of YBCO layer thickness. In Fig. 4(a) we show the variation of T_c as a function of d_Y in LSMO-YBCO-LSMO trilayers. In

order to estimate the effects of magnetic boundaries on T_c , we have also measured the superconducting transition temperature of PBCO-YBCO-PBCO trilayers. Results of these measurements are also shown in Fig. 4(a). For this non-magnetic system, the T_c drops as the thickness of the YBCO layer (d_Y) is reduced. The variation of T_c with d_Y in PBCO-YBCO-PBCO multilayers has been studied extensively by several groups, and various reasons have been given for the drop^{33,34,35}. These include interfacial stress, a drop in c-axis coupling of the condensate as the number of CuO₂ planes is reduced etc. However, the effect of uniaxial stress applied along the a-axis and b-axis of the YBCO crystal on its T_c is nearly equal and opposite³⁶. This result rules out any direct effect of the lattice mismatch induced stress on T_c . However, Varela et al³⁴ have shown that the overall stress pattern also gives rise to very significant and non-uniform changes within YBCO unit cell, which may reduce the hole concentration in the CuO₂ planes located close to the interfaces. We may write this interface driven reduction in T_c as $\Delta T_c(d_Y)_{interface}$. Since the lattice parameters of La_{0.67}Sr_{0.33}MnO₃ and PrBa₂Cu₃O₇ are identical within 0.5%, we assume the effect of the interface on T_c to be similar for YBCO films sandwiched between the LSMO layers. The LSMO layers, however, also affect the T_c through pair-breaking. We can therefore argue that the larger drop in T_c of LSMO-YBCO-LSMO trilayers of a given d_Y as compared to the T_c of PBCO-YBCO-PBCO of the same d_Y is due to the magnetic pair-breaking effects. A rigorous treatment of pair breaking effects of a ferromagnetic film deposited on top of a superconductor requires solution of the Usadel equation for different degree of interface transparency for Cooper pair tunneling^{37,38}.

C. Magnetic coupling in LSMO - YBCO - LSMO trilayers:

Having established the existence of ferromagnetic and superconducting orders in these trilayers, we now discuss the behavior of interlayer magnetic coupling between the LSMO layers separated by YBCO below and above the T_c . Fig. 5 shows a series of M-H loops of an LSMO-YBCO-LSMO trilayer with $d_Y = 100$ Å taken at various temperatures with the external magnetic field aligned along [100] direction. In the loops measured at $T > 100$ K, one can easily identify a critical field $|H_s|$ up to which the magnetic moment of the trilayer remains close to zero, and then quickly achieves the saturation value once the field $|H|$ exceeds $|H_s|$. The magnetization of the sample below the superconducting transition drops rapidly at low fields because of the diamagnetic signal from the YBCO layer. The reverse branch of the hysteresis loops shows a large irreversibility due to pinning of the magnetic flux. However, the ferromagnetic component of the magnetization is also found to persist in the superconducting state. A careful look at the magnetizing

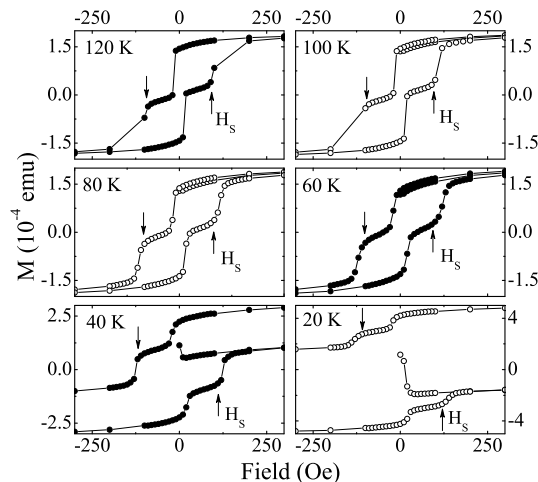


FIG. 5: Low-field section of isothermal hysteresis loops of a LSMO-YBCO-LSMO trilayer with 100 Å YBCO interlayer, measured at 20, 40, 60, 80, 100, and 120 K. All measurements were performed on zero-field-cooled samples and with in-plane applied field along the [100] direction. The switching field has been marked as H_s (see text for details).

branches of Panels c, d and e clearly reveals the characteristic field H_s below which the magnetization remains nearly constant. A similar behavior of the hysteresis, both above and below T_c , is seen in trilayers with a different YBCO layer thickness. The M-H loops of some samples at 100 K are shown in Fig. 6.

A straightforward explanation for the existence of H_s can be given by invoking antiferromagnetic exchange coupling between the LSMO layers separated by normal and superconducting YBCO. Earlier measurements of magnetization in superlattices of ferromagnetic manganites and non-magnetic but metallic LaNiO_3 have revealed indirect coupling mediated by the conduction electrons of the spacer^{6,7}. This coupling is oscillatory with the thickness of the spacer. However, before proposing such fundamental mechanism, we must rule out some rather mundane processes, which could lead to a similar effect. First of all, the interfaces of perovskite oxides based multilayers have an inherent stereochemical disorder even when they are atomically sharp³⁹. This disorder is caused by a change in the nearest neighbor environment of the magnetically active ions, and can lead to random pinning of their moment. While a gradual depinning of these moments with the increasing field would lead to deviations from a square hysteresis loop typical of a soft magnet such as LSMO, it is not likely to result in the M-H loops seen in Figs. 5 and 6. One may also argue that the uncompensated copper spins at the interface help stabilize this random state. In order to rule out these possibilities, we have measured the M-H loops of LSMO-PBCO-LSMO trilayers. In Fig. 7(a, b and c) we compare the magnetization curves of

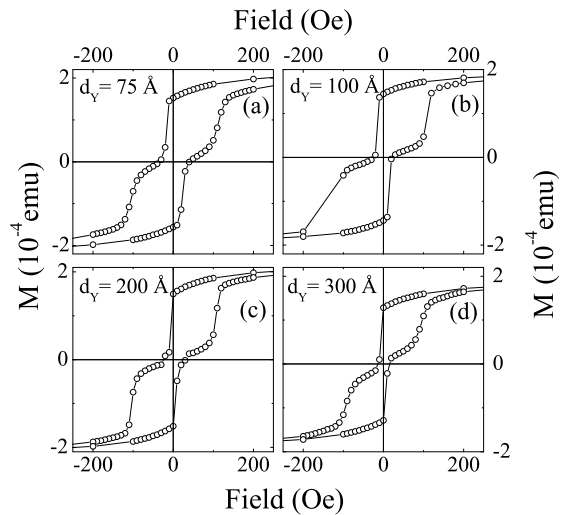


FIG. 6: Panels 'a', 'b', 'c' and 'd', display the results of isothermal magnetization measurements at 100 K for trilayers with 75, 100, 200 and 300 Å thick YBCO interlayer, respectively. The measurement field was directed along the [100] direction in the plane of the trilayers. The low field region is magnified in order to emphasize the antiferromagnetic coupling between the LSMO layers below 200 Oe.

a 600 Å thick single layer LSMO film, a LSMO-PBCO-LSMO trilayer and a LSMO-YBCO-LSMO trilayer. In all three cases the measuring field was along the [100] direction. Fig. 7(d) shows the M-H loop of the LSMO-YBCO-LSMO trilayer measured with $H \parallel [110]$ for comparison. It is evident

from these data that the hysteresis with the characteristic magnetizing field H_s is seen only in the case of LSMO-YBCO-LSMO trilayers. This observation rules out the role of uncompensated copper spins, as these factors are present in LSMO-PBCO-LSMO as well. Some signatures of the type of M-H curve seen in Figs. 5 and 6, have also been observed by Przysłupski et al.²⁰ in $\text{La}_{0.67}\text{Sr}_{0.33}\text{MnO}_3 - \text{YBa}_2\text{Cu}_3\text{O}_7$ superlattices with thin (~ 60 Å) LSMO layers. They have presented a scenario where migration of holes from the YBCO into the LSMO converts a few unit cells of the latter into an antiferromagnet. This AF ordered layer pins the magnetic moment of the remaining ferromagnetic portion. Since the LSMO layer is on both sides of the YBCO, this effect should lead to two pinned magnetization vectors whose relative orientation can be anywhere from 0 to 180°. However, the observation of a net zero magnetization at $H < |H_s|$ demands that this angle is 180°. This is possible only when there is an exchange coupling across the YBCO. The magnetic behavior of ferromagnetic and antiferromagnetic LSMO couples has been studied in detail by Izumi et al.⁴⁰, for the case of $\text{La}_{0.6}\text{Sr}_{0.4}\text{MnO}_3 / \text{La}_{0.45}\text{Sr}_{0.55}\text{MnO}_3$ superlattices, where the latter compound is a metallic A-type antiferromagnet. The Mn

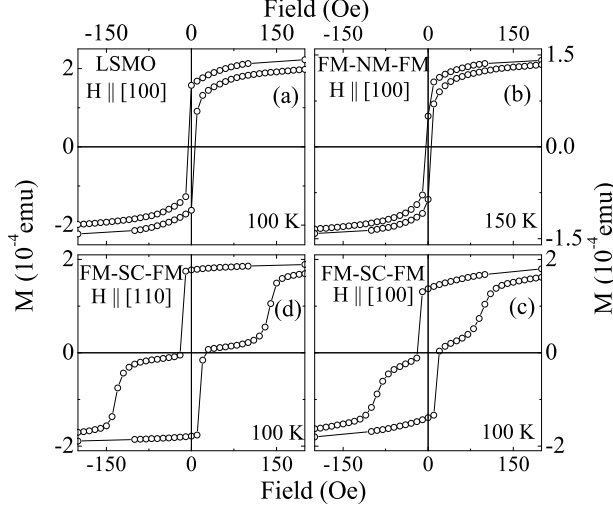


FIG. 7: A comparative view of the magnetization behavior of a 600 Å LSMO film (panel ‘a’), LSMO-PBCO-LSMO trilayer with 300 Å PBCO (panel ‘b’) and LSMO-YBCO-LSMO trilayer with 300 Å YBCO (panel ‘c’). The external magnetic field was in the plane of the film and directed along the [100] axis. Panel ‘d’ shows the magnetization while the field was applied along the [110] direction for the LSMO-YBCO-LSMO trilayer. All the curves were corrected for a small diamagnetic response of the substrate.

spins in alternate layers of this compound are coupled antiferromagnetically with their orientation in the [001] plane. Izumi et al.⁴⁰ note that the magnetization of the ferromagnetic layers is perpendicular to the magnetic easy axis of the antiferromagnetic layer, thus ruling out exchange biasing. While the measurement of far infrared conductivity $\sigma_1(\omega)$ of YBCO-LSMO multilayers by Holden et al.⁴¹ do show a strong suppression of the free-carrier contribution to $\sigma_1(\omega)$, migration of holes is only one of the possible mechanisms proposed by them for the suppression. Further, keeping in view the result of Izumi et al.⁴⁰, a possible hole transfer does not *a priori* imply exchange biasing. In order to check if there is any exchange biasing effect of the interfacial LSMO in our trilayers, we have plotted a minor loop for a sample with $d_Y = 100$ Å. Starting from saturation magnetization in the forward direction, the field was decreased to a value $|H| < |H_s|$ in the negative direction and then increased again. In the presence of exchange biasing, the minor loop obtained in this way should be shifted along the field axis by an amount equal to the biasing field. However, the minor loop in Fig. 8 shows no shift within an accuracy of 5 Oe.

Noting that the hysteresis seen in Figs. 6 and 7 is a signature of antiferromagnetic coupling between the LSMO layer magnetizations, we now proceed to estimate the exchange energy and its temperature dependence. The free energy expression for two magnetic layers of equal thick-

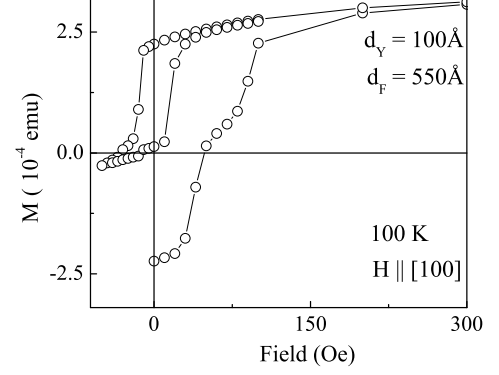


FIG. 8: The minor hysteresis loop (see text for details) of a trilayer with 100 Å YBCO layer sandwiched between 550 Å LSMO layers on both sides, is shown superposed on the main magnetization curve. The measurement was performed at 100 K after cooling the sample in zero-field.

ness coupled by bilinear coupling can be written as⁴²,

$$F = F_c + F_a - \vec{H} \cdot (\vec{M}_1 + \vec{M}_2)t \quad (2)$$

where \vec{M}_1 and \vec{M}_2 are the magnetizations of the top and bottom LSMO layers, F_c is the coupling energy per unit area, and t the thickness of one LSMO layer. The anisotropy energy F_a derives contributions from the magnetocrystalline anisotropy as well as in-plane uniaxial anisotropy of the film. Under the assumption of a bilinear coupling, F_c can be written as;

$$F_c = -J_1(\widehat{M}_1 \cdot \widehat{M}_2) \quad (3)$$

Here \widehat{M}_1 and \widehat{M}_2 are unit magnetization vectors, and $J_1 < 0$ corresponds to antiferromagnetic coupling between the FM layers. The equilibrium orientation of \vec{M}_1 and \vec{M}_2 are found by minimization of the free energy with respect to variations in the orientations of these two vectors. In a special case, when the interlayer exchange $J_1(\widehat{M}_1 \cdot \widehat{M}_2)$ is $< F_a$, the magnetization increases slowly in small field and then at a critical value of the field jumps to the saturation M_s . The switching field H_s in this case for magnetic layers of equal thickness (t), and magnetization density (M_s) is written as;

$$H_s = -(J_1/M_s t) \quad (4)$$

The behavior of magnetization seen in Figs (5, 6, and 7) corresponds to this situation. We have made an estimate of J_1 from the measured H_s and magnetization density M_s using Eq. 4. Fig. 9 shows the variation of J_1 as a function of temperature for trilayers of different YBCO layer thickness. In the figure we note that the coupling energy at $T > T_c$ is small, non-oscillatory and decreases

exponentially with the thickness of the superconductor. In all cases however, J_1 increases monotonically as the temperature is lowered to T_c . Below this temperature a truncation of the monotonic growth of J_1 is evident in all samples.

The temperature dependence of the interlayer exchange coupling in metallic multilayers has been worked out theoretically^{43,44}. Following Bruno⁴⁴, the amplitude of the linear exchange coupling coefficient J_1 increases with the decreasing temperature in the following manner,

$$J_1(T) = J_1(0) \left(\frac{T/T_0}{\sinh T/T_0} \right) \quad (5)$$

where the characteristic temperature T_0 depends on Fermi wave-vector k_F and spacer thickness d_n through the relation $T_0 = \hbar k_F / 2\pi k_B d_n m$, where m is the free electron mass and \hbar and k_B are Planck and Boltzmann constants, respectively. The calculations of Edwards et al.⁴³ also yield a similar temperature dependence of J_1 . Since the transport in the present case is along the c -axis of the YBCO, the relevant Fermi wave-vector is $k_{Fz} = \pi/2c$, where c is the c -axis lattice parameter (~ 12 Å)¹⁰. We have fitted the temperature dependence of J_1 shown in Fig. 9 to Eq. 5. However, the average value of k_{Fz} obtained from these fits is larger by a factor of ~ 4 compared to the k_{Fz} expected for YBCO¹⁰. In Fig. 9 we show a theoretical curve for $J_1(T)$ generated using Eq. 5 with $k_{Fz} = \pi/2c$, $d_Y = 100$ Å and $J_1(T)$ such that the experimental and calculated values of J_1 at 120 K are the same. The calculated $J_1(T)$ shows a steep increase at the lower temperatures where the experimental data reach saturation. This truncation of the theoretically expected growth of J_1 below T_c is suggestive of a superconducting gap.

IV. DISCUSSION

Although the physics of magnetic coupling across a superconducting spacer of anisotropic order parameter is an enormously complicated problem to analyze, the following arguments can be made on the basis of the data shown in Fig. 5 through Fig. 9. We first consider the case when YBCO is in the normal state. The coupling in this situation is mediated by the transport of carriers perpendicular to CuO_2 planes in these c -axis-oriented films. While the resistivity of YBCO along the c -axis shows a variety of behaviors depending on doping concentration and defect structure, for optimally doped YBCO it is metallic, but larger by a factor of ~ 50 compared to the in-plane resistivity⁴⁵. The c -axis transport in optimally doped and overdoped YBCO involves blocking of coherent interplanar tunneling by the in-plane scattering. This leads to $\rho_c \propto \rho_{ab}$ ^{46,47}. In underdoped systems diffusive tunneling dominates the transport, leading to a semiconductor like resistivity⁴⁸. The non-oscillatory and

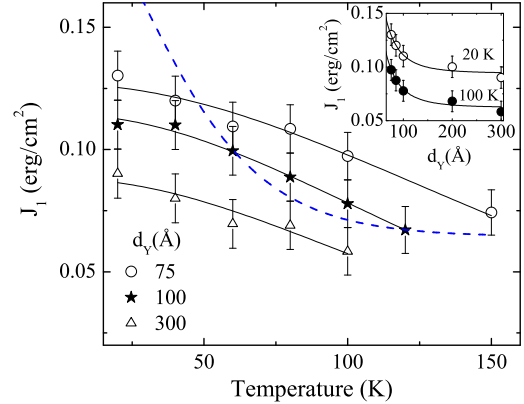


FIG. 9: The antiferromagnetic coupling energy (J_1) calculated using the relation $|J_1| = H_s M_s t$ (Eq. 4), is shown as a function of temperature for three sandwich structures with YBCO thickness of 75 Å (O), 100 Å (*), and 300 Å (Δ) and a constant LSMO thickness of 300 Å. The solid lines are fits to the equation $J_1 \sim (T/T_0)/\sinh(T/T_0)$ (Ref. 44). Dashed line is a theoretically generated curve showing how J_1 should grow with respect to the value at 120 K if k_{Fz} is taken to be $\pi/2c$, where c is the c -axis lattice parameter (see text for details). Inset: The dependence of J_1 on the thickness of the YBCO spacer is plotted at 20 K and 100 K. A characteristic decay length of ~ 150 Å was obtained by fitting these data to a first order exponentially decaying function (shown as the solid lines).

predominantly antiferromagnetic IEC seen here is analogous to the behavior of exchange coupling in Fe-FeSi-Fe⁴⁹ and Fe-Si-Fe⁵⁰ heterostructures. The IEC in this case is strongly antiferromagnetic ($J_1 \sim 2$ erg/cm²) for a thin spacer, and decays exponentially with the increasing spacer thickness. Furthermore, the exchange energy J_1 shows a monotonic drop with the increasing temperature, a behavior similar to the data shown in Fig. 9. A bias towards antiferromagnetic IEC has been predicted theoretically as well. Shi, Levy and Fry⁵¹ have shown that this bias for AF-coupling arises from a competition between the RKKY-like exchange and superexchange, and a non-cancellation of the non-oscillatory parts of these two contributions. An AF coupling, which decays exponentially with the spacer thickness, has been predicted by Slonczewski⁵² and Bruno⁴⁴ using an electron tunneling picture. The theory⁴⁴ predicts a d_n dependence of the type $J_1 \sim (1/d_n^2) \exp(-d_n/\lambda)$. The calculated value of the coupling energy J_1 for our trilayers is plotted in the inset of Fig. 9 as a function of the spacer layer thickness. We have fitted these data to a first-order exponential decay of the type given by Bruno et al.⁴⁴. Result of this fitting is shown as solid-lines in the inset. The characteristic decay length λ inferred from the fit is ~ 150 Å. Since the c -axis transport in YBCO is controlled by a delicate balance between single electron tunneling and

intralayer electron - electron scattering processes^{46,47,48}, a tunneling picture for IEC is applicable, albeit with the caveat that it is unlike the tunneling through a semiconducting barrier where thermally induced carriers can enhance IEC at higher temperatures⁴⁴. The IEC in this case is expected to decay with temperature as the c-axis resistivity shows a linear temperature dependence.

The truncation of the monotonic growth of the exchange coupling energy when the YBCO layer becomes superconducting (as seen in Fig. 9) is in agreement with the predictions of Šipr and Györfy⁸, and of de Melo⁹. However, the extent of the drop in the coupling energy in the $T = 0$ limit depends on the strength of the superconducting gap parameter. For a weak ferromagnet and an isotropic superconductor, de Melo⁹ has derived an analytic expression for the effective coupling Hamiltonian;

$$H_{eff} \sim \frac{\cos(2k_F d_s)}{(2k_F d_s)^2} \exp\left(-\frac{k_F d_s \Delta}{E_F}\right) \quad (6)$$

where, k_F and d_s are the Fermi momentum and thickness of the S-layer respectively. Δ is the superconducting gap and E_F is the Fermi energy. This expression shows that the superconducting order does not actually contribute to the oscillating part of the interaction, it only induces a relative decrease in the strength of interaction as compared to the interaction for a normal metallic spacer. However, the low temperature calculations in Refs. 8 and 9 are valid only for an isotropic gap parameter. de Melo has recently considered the case of IEC through a d-wave superconductor whose order parameter lies in the plane of the multilayer¹⁰. The main contribution to coupling in this case comes from the wave vectors connecting points at the Fermi surface along the [001] direction and for $\vec{k}_{||}$ lying along the direction of nodes. A distinct

suppression, although not as much as in the case of a fully gapped system, has been seen in the superconducting state.

V. CONCLUSIONS

In summary, we have studied the magnetic and superconducting states of epitaxial thin film heterostructures consisting of two $\text{La}_{0.67}\text{Sr}_{0.33}\text{MnO}_3$ layers separated by a layer of $\text{YBa}_2\text{Cu}_3\text{O}_7$, whose c-axis is perpendicular to the plane of the heterostructure. We see a distinct influence of the ferromagnetic boundaries on the T_c of the YBCO layer. This is attributed to the pair-breaking phenomena near the F-S interface. The hysteresis loops for in-plane magnetization of the heterostructures show signatures of an antiferromagnetic coupling between the moments of the two LSMO layers in the superconducting as well as the normal state of the spacer. The temperature dependence of the exchange coupling energy shows a monotonic growth followed by saturation on lowering the temperature. The long range coupling was found to decrease exponentially with the increasing thickness of the spacer layer. The suppression of J_1 at $T < T_c$ suggests inhibition of single electron tunneling along the c-axis of YBCO as the in-plane superconducting order parameter becomes non-zero.

Acknowledgments

This research has been supported by a grant from the Defense Research and Development Organization, Government of India, and the internal funding of I.I.T. Kanpur.

* Electronic address: rcb@iitk.ac.in

¹ See, for example, *Ultrathin Magnetic Structures II*, ed. B. Heinrich and J. A. C. Bland, (Springer-Verlag, Berlin, 1994).

² P. Grunberg, R. Schreiber, Y. Pang, M. B. Brodsky, and H. Sowers, Phys. Rev. Lett. **57**, 2442 (1986).

³ M. N. Baibich, J. M. Broto, A. Fert, F. N. Van Dau, F. Petroff, P. Eitenne, G. Creuzert, A. Friederich, and J. Chazelas, Phys. Rev. Lett. **61**, 2472 (1988).

⁴ S. S. P. Parkin, N. More, and K. P. Roche, Phys. Rev. Lett. **64**, 2304 (1990).

⁵ A. Orozco, S. B. Ogale, Y. H. Li, P. Fournier, Eric Li, H. Asano, V. Smolianinova, R. L. Greene, R. P. Sharma, R. Ramesh, and T. Venkatesan, Phys. Rev. Lett. **83**, 1680 (1999).

⁶ K. R. Nikolaev, A. Yu. Dobin, I. N. Krivorotov, W. K. Cooley, A. Bhattacharya, A. L. Kobrinskii, L. I. Glazman, R. M. Wentzovitch, E. Dan Dahlberg, and A. M. Goldman, Phys. Rev. Lett. **85**, 3728 (2000).

⁷ P. Padhan, R. C. Budhani, and R. P. S. M. Lobo, Euro-

phys. Lett **63**, 771 (2003).

⁸ O. Šipr and B. L. Györfy, J. Phys: Condens. Matter **7**, 5239 (1995).

⁹ C. A. R. Sá de Melo, Phys. Rev. Lett. **79**, 1933 (1997); Phys. Rev. B **62**, 12303 (2000).

¹⁰ C. A. R. Sá de Melo, Physica C **387**, 17 (2003).

¹¹ J. J. Hauser, H. C. Theuerer, and N. R. Werthamer, Phys. Rev. **142**, 118 (1966).

¹² H.-U. Habermeier, G. Cristiani, R. K. Kremer, O. Lebedev, and G. van Tendeloo, Physica C **364-365**, 298 (2001).

¹³ Z. Sefrioui, D. Arias, V. Peña, J. E. Villegas, M. Varela, P. Prieto, C. León, J. L. Martinez, and J. Santamaria, Phys. Rev. B **67**, 214511 (2003).

¹⁴ B. S. H. Pang, R. I. Tomov, and M. G. Blamire, Supercond. Sci. Technol. **17**, 624 (2004).

¹⁵ Z. W. Dong, R. Ramesh, T. Venkatesan, M. Johnson, Z. Y. Chen, S. P. Pai, V. Talyanski, R. P. Sharma, R. Shreekala, C. J. Lobb, and R. L. Greene, Appl. Phys. Lett. **71**, 1718 (1997).

¹⁶ A. M. Goldman, V. Vasko, P. Kraus, K. Nikolaev, and V.

- A. Larkin, J. Mag. Mag. Mater. 200, **69** (1999).
- ¹⁷ N. C. Yeh, R. P. Vasquez, C. C. Fu, A. V. Samoilov, Y. Li, and K. Vakili, Phys. Rev. B **60**, 10522 (1999).
 - ¹⁸ G. Jacob, V. V. Moshchalkov, and Y. Bruynseraede, Appl. Phys. Lett. **66**, 2564 (1995).
 - ¹⁹ L. Fábrega, R. Rubi, V. Vrtik, C. Ferrater, F. Sánchez, M. Varela, and J. Fontcuberta, J. Magn. Magn. Mater. **211**, 180 (2000).
 - ²⁰ P. Przyslupski, I. Komissarov, W. Paszkowicz, P. Dłuzewski, R. Minikayev, and M. Sawicki, Phys. Rev. B **69**, 134428 (2004).
 - ²¹ Yan. Wu, Y. Suzuki, U. Rüdiger, J. Yu, A. D. Kent, T. K. Nath, and C. B. Eom, Appl. Phys. Lett. **75**, 2295 (1999).
 - ²² H. Y. Zhai and W. K. Chu, Appl. Phys. Lett. **76**, 3469 (2000).
 - ²³ M. Kawasaki, K. Takahashi, T. Maeda, R. Tsuchiya, M. Shinohara, O. Ishiyama, T. Yonezawa, M. Yoshimoto, and H. Koinuma, Science **266**, 1540 (1994).
 - ²⁴ K. Senapati and R. C. Budhani, Phys. Rev. B **70**, 174506 (2004).
 - ²⁵ K. Senapati, S. Chakravarty, Leena K. Sahoo, and R. C. Budhani, Rev. Sci. Instrum. **75**, 141 (2004).
 - ²⁶ C. Kittel, *Introduction to Solid State Physics – 7th Edition* (John Wiley and Sons – New York 1996), p. 448.
 - ²⁷ G. S. Rushbrooke and P. J. Wood, Mol. Phys. **1**, **257** (1958).
 - ²⁸ Y. Suzuki, H. Y. Hwang, S-W. Cheong, and R. B. van Dover, Appl. Phys. Lett. **71**, 140 (1997).
 - ²⁹ K. Steenbeck and R. Hiergeist, Appl. Phys. Lett. **75**, 1778 (1999).
 - ³⁰ A. M. Haghir-Gosnet, J. Wolfman, B. Mercey, Ch. Simon, P. Lecœur, M. Korzenski, M. Hervieu, R. Desfeux, and G. Baldinozzi, J. Appl. Phys. **88**, 4257 (2000).
 - ³¹ K. Steenbeck, T. Habisreuther, C. Dubourdieu, and J. P. Sénateur, Appl. Phys. Lett. **80**, 3361 (2002).
 - ³² A. Urushibara, Y. Moritomo, T. Arima, A. Asamitsu, G. Kido, and Y. Tokura, Phys. Rev. B **51**, 14103 (1995).
 - ³³ J. -M. Triscone and Ø. Fischer, Rep. Prog. Phys. **60**, 1673 (1997), and references therein.
 - ³⁴ M. Varela, Z. Sefrioui, D. Arias, M. A. Navacerrada, M. Lucía, M. A. López de la Torre, C. León, G. D. Loos, F. Sánchez-Quesada, and J. Santamaría, Phys. Rev. Lett. **83**, 3936 (1999).
 - ³⁵ T. Terashima, K. Shimura, Y. Bando, Y. Matsuda, A. Fujiyama, and S. Komiyama, Phys. Rev. Lett. **67**, 1362 (1991).
 - ³⁶ W. E. Pickett, Phys. Rev. Lett. **78**, 1960 (1997).
 - ³⁷ Z. Radovic, M. Ledvij, L. Dobrosavljevic, A. I. Buzdin, and J. R. Clem, Phys. Rev. B **44**, 759 (1991).
 - ³⁸ L. Lazar, K. Westerholt, H. Jabel, L. R. Tagirov, Yu. V. Goryunov, N. N. Garifyanov, and I. A. Garifullin, Phys. Rev. B **61**, 3711 (2000).
 - ³⁹ P. Padhan and R. C. Budhani (unpublished).
 - ⁴⁰ M. Izumi, T. Manako, Y. Konishi, M. Kawasaki, and Y. Tokura, Phys. Rev. B **61**, 12187 (2000).
 - ⁴¹ Todd Holden, H.U. Habermeier, G. Cristiani, A. Golnik, A. Boris, A. Pimenov, J. Hummelcek, O. Lebedev, G. Van Tendello, B. Keimer, and C. Bernhard, Phys. Rev. B **69**, 064505 (2004).
 - ⁴² S. O. Demokritov, J. Phys. D: Appl. Phys. **31**, 925 (1998).
 - ⁴³ D. M. Edwards, J. Mathon, R. B. Muniz, and M. S. Phan, Phys. Rev. Lett. **67**, 493 (1991).
 - ⁴⁴ P. Bruno, Phys. Rev. B **52**, 411 (1995).
 - ⁴⁵ S. L. Cooper and K. E. Gray, in Physical properties of High Temperature superconductors IV, ed. D. M. Ginzburg (World Scientific, Singapore 1994) pp 61-188.
 - ⁴⁶ N. Kumar and A. M. Jayannavar, Phys. Rev. B **45**, 5001 (1992).
 - ⁴⁷ M. S. Kumar, S. Duttagupta, and N. Kumar, Phys. Rev. B **65**, 134501 (2004).
 - ⁴⁸ M. Turlakov and A. J. Leggett, Phys. Rev. B **63**, 064518 (2001).
 - ⁴⁹ J. J. de Vries, J. Kohlhepp, F. J. A. den Broeder, R. Coehoorn, R. Jungblut, A. Reinders, and W. J. M. de Jonge, Phys. Rev. Lett. **78**, 3023 (1997).
 - ⁵⁰ G. J. Strijkers, J. T. Kohlhepp, H. J. N. Swagten, and W. J. M. de Jonge, Phys. Rev. Lett. **84**, 1812 (2000).
 - ⁵¹ Z. P. Shi, P. M. Levy, and J. L. Fry, Phys. Rev. B **49**, 15159 (1994).
 - ⁵² J. C. Slonczewski, Phys. Rev. B **39**, 6995 (1989).